

RESEARCH

Open Access



# Silencing HOXC13 exerts anti-prostate cancer effects by inducing DNA damage and activating cGAS/STING/IRF3 pathway

Maozhang Li<sup>1,2†</sup>, Guangwei Bai<sup>2†</sup>, Yi Cen<sup>3†</sup>, Qitong Xie<sup>2</sup>, Jiahong Chen<sup>2</sup>, Jia Chen<sup>2</sup>, Qingbiao Chen<sup>4</sup>, Weide Zhong<sup>1\*</sup>  and Xiaobo Zhou<sup>2\*</sup>

## Abstract

**Background** Advanced prostate cancer (PCa) will develop into castration-resistant prostate cancer (CRPC) and lead to poor prognosis. As the primary subtype of CRPC, CRPC-AR accounts for the major induction of PCa heterogeneity. CRPC-AR is mainly driven by 25 transcription factors (TFs), which we speculate may be the key factors driving PCa toward CRPC. Therefore, it is necessary to clarify the key regulator and its molecular mechanism mediating PCa progression.

**Methods** Firstly, we downloaded transcriptomic data and clinical information from TCGA-PRAD. The characteristic gene cluster was identified by PPI clustering, GO enrichment, co-expression correlation and clinical feature analyses for 25 TFs. Then, the effects of 25 TFs expression on prognosis of PCa patients was analyzed using univariate Cox regression, and the target gene was identified. The expression properties of the target gene in PCa tissues were verified using tissue microarray. Meanwhile, the related mechanistic pathway of the target gene was mined based on its function. Next, the target gene was silenced by small interfering RNAs (siRNAs) for cellular function and mechanistic pathway validation. Finally, CIBERSORT algorithm was used to analyze the infiltration levels of 22 immune cells in PCa patients with low and high expression of target gene, and validated by assaying the expression of related immunomodulatory factor.

**Results** We found that HOX family existed independently in 25 TFs, among which HOXC10, HOXC12 and HOXC13 had unique clinical features and the PCa patients with high HOXC13 expression had the worst prognosis. In addition, HOXC13 was highly expressed in tumor tissues and correlated with Gleason score and pathological grade. In vitro experiments demonstrated that silencing HOXC13 inhibited 22RV1 and DU145 cell function by inducing cellular DNA damage and activating cGAS/STING/IRF3 pathway. Immune infiltration analysis revealed that high HOXC13 expression suppressed infiltration of  $\gamma\delta$  T cells and plasma cells and recruited M2 macrophages. Consistent with these results, silencing HOXC13 up-regulated the transcriptional expression of IFN- $\beta$ , CCL2, CCL5 and CXCL10.

<sup>†</sup>Maozhang Li, Guangwei Bai and Yi Cen have equally contributed to this work.

\*Correspondence:  
Weide Zhong  
zhongwd2009@live.cn  
Xiaobo Zhou  
13829969092@139.com

Full list of author information is available at the end of the article



**Conclusion** HOXC13 regulates PCa progression by mediating the DNA damage-induced cGAS/STING/IRF3 pathway and remodels TIME through regulation of the transcription of the immune factors IFN- $\beta$ , CCL2, CCL5 and CXCL10.

**Keywords** Prostate cancer, HOXC13, cGAS/STING/IRF3 pathway, IFN- $\beta$ , Immune infiltration

## Introduction

Prostate cancer (PCa) is one of the most common malignant tumors of the male genitourinary system and the second leading cause of cancer death in men [1, 2]. PCa has androgen-dependent growth characteristics, androgen deprivation therapy (ADT) is the primary treatment for this type of patients [3]. However, after an average of two years with ADT, most patients progress to castration-resistant prostate cancer (CRPC), implying that ADT is ineffective for PCa and tumors can grow in a hypoandrogenic environment [4]. CRPC has a highly heterogeneous clinical course [5]. Patients with painless disease can survive for years without progression, while aggressive disease can rapidly metastasize and become incurable. Although the incidence of PCa has generally decreased in recent years, a steady increase in the incidence of metastatic CRPC has been observed, which suggests a change in treatment strategy [6]. Therefore, it is necessary to further reveal the formation mechanisms of CRPC heterogeneity, for which tumor subtypes may provide valuable molecular information.

Today, high-throughput sequencing for epigenomics provides potent technical support for studying tumor heterogeneity, revealing the heterogeneity among tumor cells and the complexity of the tumor microenvironment (TME) [7]. In a recent study, researchers using assay for transposase-accessible chromatin sequencing (ATAC-seq) combined with RNA sequencing (RNA-seq) on 22 organoids, 6 patient-derived xenografts and 12 cell lines revealed that CRPC consists of four molecular subtypes, with CRPC-AR as the primary subtype driven by 25 key TFs (AR, FOXA1, PGR, FOXO3, FOXB2, FOXK1, GATA2, FOXO4, HOXA13, HOXB13, FOXJ2, HOXC12, FOXN3, NFYB, FOXP3, FOXL2, NFIC, HOXC13, FOXC2, FOXS1, HSF4, ARID5A, HNF1B, HOXC10 and HNF1A) [8]. These 25 TFs have important regulatory roles in PCa progression, among which FOXA1, FOXK1, GATA2, HOXA13 and FOXC2 have been proven to be oncogenic, while FOXO3, HOXB13, FOXP3 and HNF1B have opposite effects [9–17]. The aberrant functional properties of these TFs in PCa suggest that they are key drivers of TME heterogeneity. TME is a complex environment filled with various cell subtypes, including tumor cells, blood vessels, immune cells and stromal cells, of which tumor immune microenvironment (TIME) is the most important component [18]. Numerous studies have demonstrated that TIME play an important role in

the physiological regulation of acquired drug resistance and anti-apoptosis in tumors [19–21]. Therefore, whether these TFs mediate alterations in TIME to affect PCa progression aroused our research interest.

We focused on 25 TFs and analyzed their expression properties and clinical features in PCa by bioinformatics to uncover the key regulator driving PCa progression. The molecular mechanism mediating PCa function was further explored by in vitro experiments. The effects of the target gene on TIME alterations were analyzed by immune infiltration. Our study may provide a novel molecular target for PCa therapy and guide clinical therapeutic decision.

## Materials and methods

### Data collection and processing

RNA-seq expression profiles of 498 prostate adenocarcinoma (PRAD) samples and 52 paracancerous samples were downloaded from The Cancer Genome Atlas (TCGA) database (<https://portal.gdc.com>), and the corresponding clinical information for TCGA-PRAD cohort was obtained from cBio Cancer Genomics Portal (cBioPortal) database (<http://cbioportal.org>). For RNA-seq expression profiles, the data type we downloaded was fragments per kilobase per million (FPKM), which was converted to transcripts per million (TPM) expressed as  $\log_2$  (TPM + 1) for subsequent analysis.

### Gene differential expression analysis

Gene expression levels in normal and tumor tissues were compared according to  $\log_2$  (TPM + 1). Further, TCGA-PRAD cohort was divided into two groups based on Gleason score (GS, < 8 vs.  $\geq$  8), tumor stage (T stage, T1–T2 vs. T3–T4), lymph node stage (N stage, N0 vs. N1) and metastasis stage (M stage, M0 vs. M1) to compare the gene expression levels under different clinical features. The statistical difference of two groups was compared by Wilcoxon test without normal distribution. The analysis method and R package (ggplot2) were implemented by R v4.0.3 software.  $P < 0.05$  was considered statistically significant.

### Protein–protein interaction (PPI) analysis

PPI for multiple proteins was analysed using String database (<https://cn.string-db.org/>). Active interaction sources for PPI include textmining, experiments, databases, co-expression, neighbourhood, gene fusion

and co-occurrence, and the interaction score was set to 0.4 (medium confidence). Further, k-means clustering method was applied to cluster multiple proteins to find characteristic protein clusters.  $P < 0.05$  was considered statistically significant.

#### Gene ontology (GO) enrichment analysis

GO terms in biological processes, molecular functions and cellular components were enriched and analysed by calculating strength (enrichment index) and false discovery rate (FDR) based on PPI network counts.  $FDR < 0.05$  was considered statistically significant.

#### Co-expression correlation analysis

Based on RNA-seq expression profiles from 498 PRAD samples, Spearman's correlation analysis was used to describe correlation between quantitative variables without normal distribution. Correlation heatmap was displayed by R package (pheatmap) and implemented by R v4.0.3 software.  $P < 0.05$  was considered statistically significant.

#### Overall survival (OS) analysis

Based on 498 PRAD samples with survival information, TCGA-PRAD cohort was divided into low expression ( $n = 249$ ) and high expression ( $n = 249$ ) groups according to the median expression value of each gene. The effects of gene expression on the prognosis of PRAD patients were analysed using univariate Cox regression and log-rank test.  $P$  values and hazard ratio (HR) with 95% confidence interval (CI) were calculated and survival curves were plotted. All the analysis methods and R packages (ggplot2, forestplot and survival) were implemented by R v4.0.3 software.  $P < 0.05$  was considered statistically significant.

#### Gene-pathway correlation analysis

The marker genes in the corresponding pathway were collected and analysed by R package (GSVA), and the correlation between target gene and pathway scores was analysed by Spearman's correlation. All the analysis method and R package were implemented by R v4.0.3 software.  $P < 0.05$  was considered statistically significant.

#### Tissue microarray information

Tissue microarray (Cat No. = HProA150CS01,  $n = 150$ ; OUTDO BIOTECH, China), including 50 paracancerous tissue samples and 100 prostate tissue samples from patients with primary PCa, were available with clinicopathologic information. Patients treated with chemotherapy or radiotherapy before the surgery were excluded from this study.

#### Immune infiltration analysis

Based on RNA-seq expression profiles of 498 PRAD samples, TCGA-PRAD cohort was divided into low expression ( $n = 249$ ) and high expression ( $n = 249$ ) groups according to the median expression value of the target gene. We performed a reliable immunoscore assessment using the R software package (immunedeconv). CIBERSORT algorithm was used to calculate the enrichment score of each sample for each immune cell to compare the infiltration levels of 22 immune cells in the two groups. All the analysis methods and R packages (ggplot2 and GSVA) were implemented by R v4.0.3 software.  $P < 0.05$  was considered statistically significant.

#### Immunohistochemistry (IHC) staining

Tissues were sequentially sectioned ( $5 \mu\text{m}$ ), dewaxed ( $65^\circ\text{C}$ , 2 h), antigen repaired (sodium citrate), blocked (5% BSA), and sealed at room temperature ( $24^\circ\text{C}$ , 20 min). Primary antibodies against HOXC13 (1:100, ABclonal, China) was added and incubated overnight at  $4^\circ\text{C}$ . After adding secondary antibody and incubating at room temperature for 1 h, DAB color development, hematoxylin counterstaining, dehydration and sealing were performed successively. The positive cell rate and the degree of staining were scored by scanning imaging. Positive cell rate score: 0–10%, 1 point; 10–50%, 2 points; 50–75%, 3 points; 75–100%, 4 points. Staining degree score: no positive staining, 0 point; canary yellow, 1 point; brownish yellow, 2 points; tan, 3 points. Immune risk score (IRS) is the product of the above two scores.

#### Cell line culture

Human PCa cell lines, DU145 and 22RV1, were purchased from BNCC (Beijing, China). Cells were maintained in DMEM (Gibco, USA) with 10% FBS (Gibco, USA) and  $100 \mu\text{g}/\text{mL}$  penicillin/streptomycin (Gibco, USA) in a humidified atmosphere containing 5%  $\text{CO}_2$  at  $37^\circ\text{C}$ .

#### siRNAs construction and transfection

siRNAs specific to HOXC13 for silencing its expression (siHOXC13-1 to siHOXC13-5), including negative control (siNC), were synthesized by GENERAL BIOL (Anhui, China). Cells ( $1 \times 10^6$  cells/mL) were seeded in 6-well culture plate and transiently transfected with 2 mL OPTI-MEM medium (Gibco, USA) using siRNA transfection reagent (Santa Cruz, USA). siHOXC13-1 sequences: 5'-GG UGACGACCUGUCCUCUATT-3' (forward) and 5'-UAGAGGACAGGUCGUCAC CTT-3' (reverse). siHOXC13-2 sequences: 5'-CGUCGAAGG CUACCAGCACTT-3' (forward) and 5'-GUGCUG

GUAGCCUUCGACGTT-3' (reverse). siHOXC13-3 sequences: 5'-AGGAAUACGCGGCUAGCAATT-3' (forward) and 5'-UUGCUGACGCGGUAUUCCTT-3' (reverse). siHOXC13-4 sequences: 5'-GCCUUAUGUACGUCUAUGATT-3' (forward) and 5'-UCAUAGACGUACAUAAGGC-3' (reverse). siHOXC13-5 sequences: 5'-GAAGAAGGUGGUCAGCAAATT-3' (forward) and 5'-UUGCUGACCACCUUCUUCTT-3' (reverse). siNC sequences: 5'-UUCUCCGAACGUGUCA CGUTT-3' (forward) and 5'-ACGUGACACGUUCGGAGAATT-3' (reverse).

#### Cell proliferation assay

After transfection for 12 h, cells ( $1 \times 10^3$  cells/well) were seeded into 96-well culture plate with 100  $\mu$ L serum medium. After incubation for 6, 12, 24 and 48 h, the OD values of cells at 450 nm were detected with 10  $\mu$ L CCK-8 reagent (Beyotime, China). Calculated and plotted the cell proliferation curve based on CCK-8 method.

#### Cell apoptosis assay

After transfection for 48 h, cells were collected and the cell suspension was prepared with  $1 \times$  binding buffer and adjusted to  $1 \times 10^6$  cells/tube, then 5  $\mu$ L of Annexin V-APC and 10  $\mu$ L of 7-AAD reagent were added, vortexed and mixed, and incubated for 15 min at room temperature (24  $^{\circ}$ C) and protected from light. Finally, 485  $\mu$ L of pre-chilled  $1 \times$  binding buffer was added to each tube and resuspended, and the data were analyzed by flow cytometry with NovoExpress software.

#### Cell migration assay

After transfection for 12 h, cells ( $5 \times 10^5$  cells/well) were seeded into 6-well culture plate with 2 mL serum medium. Parallel lines were drawn at the bottom of the culture plate with the pipette tip, and the fallen cells were rinsed with PBS. The migrating cells at 0 and 48 h were imaged and the migration distances were calculated by Image J v1.8.0 software.

#### Cell invasion assay

A double cavity transmission system with an 8  $\mu$ m pore was used in this assay (the upper chamber was pre-added with 80  $\mu$ L matrix solution and incubated at 37  $^{\circ}$ C for 1 h). After transfection for 12 h, cells ( $5 \times 10^4$  cells/well) were seeded into the upper chamber of the inserts with 200  $\mu$ L serum-free medium, and the lower chamber was filled with 500  $\mu$ L serum medium. After invasion for 48 h, inserts were fixed with 100% methanol and then stained with 0.1% crystal violet (Biosharp, China). The invading cells on the inserts were imaged and counted by Image J v1.8.0.

#### Cell viability assay

Cells ( $1 \times 10^3$  cells/well) were seeded into 96-well culture plate with 100  $\mu$ L serum medium for 24 h. Then 1, 5, 10, 20, 40, 60, 80 and 100  $\mu$ M specific cGAS inhibitor RU.521 (MCE, USA) were added and cultured for 48 h, respectively. The OD values of cells at 450 nm were detected with 10  $\mu$ L CCK-8 reagent.

#### Immunofluorescence (IF) staining

Cells were fixed with 4% PFA for 15 min and permeabilized with 0.5% Triton X-100 (Sigma, USA) for 30 min. Then, dsDNA antibody (1:1000, Abcam, USA) was added to incubate the cells at 4  $^{\circ}$ C overnight. After washing three times, samples were incubated with secondary antibody-Alexa fluor 488 (1:200, Abcam, USA) for 1 h at room temperature and counterstained with DAPI (Sigma, USA). The staining was observed and imaged under fluorescence microscope.

#### Quantitative reverse transcriptase PCR (qRT-PCR) assay

Total RNA was extracted from cells and tissues using Trizol reagent (BioTeke, China). After determining the concentration and purity of RNA samples, RNA reverse transcription was performed according to the steps of reverse transcription kit (Vazyme, China). The synthetic cDNAs were used as template for fluorescence detection using SYBR Green qPCR detection kit (Biosharp, China). The reaction procedure was as follows: pre-denaturation at 95  $^{\circ}$ C for 5 min, followed by 40 cycles of denaturation at 95  $^{\circ}$ C for 30 s, annealing at 60  $^{\circ}$ C for 30 s, and extension at 72  $^{\circ}$ C for 15 s. The results were quantified using the relative quantitative  $2^{-\Delta\Delta CT}$  method. HOXC13 primer sequences: 5'-AAGGAATACGCGGCTAGCAA-3' (forward) and 5'-GGAGATGAGGCGCTTTCGAT-3' (reverse). IFN- $\beta$  primer sequences: 5'-GACG CCGCAT TGACCATCT-3' (forward) and 5'-CCTTGGCCTTCA GGTAATGCAG-3' (reverse). CCL2 primer sequences: 5'-CTCGCTCAGCCAGATGCAAT-3' (forward) and 5'-TTGGGTTTGCTTGCCAGGT-3' (reverse). CCL5 primer sequences: 5'-CCT GTATGACTCCCGGCT GAA-3' (forward) and 5'-AAGCCTCCCAAGCTA GGACA A-3' (reverse). CXCL10 primer sequences: 5'-TGCCATTCTGATTTGCTGCCTT-3' (forward) and 5'-GGACAAAATTGGCTTGCAAGGAAT-3' (reverse). ACTB primer sequences: 5'-TGGCACCAGCACAAT GAA-3' (forward) and 5'-CTAAGTCATAGTC CGC CTAGAAGCA-3' (reverse).

#### Western blot (WB) assay

Nucleoplasmic separation of cells according to the kit instruction (Beyotime, China). Cells were lysed in RIPA lysis buffer (Sigma, USA) supplemented with

0.1% protease-inhibitor (Sigma, USA). The isolated proteins (40 µg) were separated on 12% SDS gels and electrotransferred to polyvinylidene difluoride membranes. Then, incubation for 16 h with primary antibodies against AR (1:1500, CST, USA), HOXC13 (1:1000, ABclonal, China), γH2AX (1:1000, ABclonal, China), cGAS (1:1000, ABclonal, China), p(Ser366)-STING (1:1000, CST, USA), STING (1:1000, CST, USA), p(Ser386)-IRF3 (1:1000, CST, USA), IRF3 (1:1000, CST, USA), H3 (1:1000, Beyotime, China) and ACTB (1:1000, BOSTER, China). The membrane was washed and incubated in horseradish peroxidase-conjugated secondary antibody. Antibody-bound protein bands were assayed using a chemiluminescent luminol enhancer solution (YEASEN, China). The gel imaging system was used for imaging analysis.

### Statistical analysis

All experiments were performed in triplicate. Statistical analysis was performed by SPSS v18.0 software. Experimental data were presented as mean ± standard deviation (SD). Comparison between multiple groups was made using one-way ANOVA (Tukey's posthoc test).  $P < 0.05$  was considered statistically significant.

## Results

### Gene cluster (HOXC10, HOXC12 and HOXC13) with unique clinical features in PCa

To understand the expression properties of 25 TFs in PCa and their correlation with clinical features, we used bioinformatics to comprehensively analyze their role in PCa progression. We found that 25 TFs were aberrantly expressed in PCa, with FOXA1, FOXB2, FOXL2, FOXP3, FOXS1, HOXB13, HOXC12, HOXC13 and HSF4 being highly expressed in tumor tissues, while ARID5A, FOXJ2, FOXN3, FOXO4, HOXA13, HOXC10, NFIC, NFYB and PGR were lowly expressed (Fig. 1A). PPI analysis of 25 TFs revealed that they could be classified into three clusters, with close interaction between green cluster (AR, ARID5A, FOXA1, FOXJ2, FOXL2, FOXN3, GATA2, HNF1A, HNF1B, HOXA13, HOXB13, HSF4, NFIC and PGR) and red cluster (FOXB2, FOXC2, FOXK1, FOXO3, FOXO4, FOXP3, FOXS1 and NFYB), while blue cluster (HOXC10, HOXC12 and HOXC13) was independent, suggesting that blue cluster may have a unique regulatory pattern in PCa progression (Fig. 1B). Functional enrichment revealed that 25 TFs were mainly enriched in nuclear chromatin and involved in positive or negative transcriptional regulation of genes (Fig. 1C). Further analysis revealed that the expression of 25 TFs was almost positively correlated, with FOXA1 being the most strongly correlated with HOXB13, in addition to HOXC12 being highly positively correlated with

HOXC13 in the blue cluster (Additional file 1: Fig. S1). Clinical features demonstrated that 25 TFs were aberrantly expressed in different pathological states, among which HOXC12 and HOXC13 were highly expressed in advanced T stage and M stage, but not with N stage (Fig. 2B–D). HOXC13 was also highly expressed in high GS (Fig. 2A). These results suggest a potential regulatory role for gene cluster (HOXC10, HOXC12 and HOXC13) in PCa progression.

### High HOXC13 expression has a worse prognosis for PCa patients

Further, we analyzed the effects of 25 TFs on OS of PCa patients. Prognostic analysis showed that FOXB2, HOXC12, FOXP3, HOXC13, FOXS1 and HSF4 were risk factors for PCa, while PGR and NFIC were protective factors (Fig. 3A). Although both HOXC12 and HOXC13 were risk factors for PCa, patients with high HOXC13 expression have a worse prognosis (Fig. 3B and C). Next, we analyzed the expression properties of HOXC13 in PCa using tissue microarray. IHC staining showed that HOXC13 was highly expressed in tumor tissues compared to paracancerous tissues and was also highly expressed in tumor tissues with high GS (Fig. 4A and B). Further classifying PCa patients into five categories (stage I to stage V) based on pathological grade, we found that HOXC13 was highly expressed in patients with high stage, and interestingly, HOXC13 was most highly expressed in patients with stage IV (Fig. 4C and D). Since the HOX family is widely involved in cellular DNA repair pathways, we analyzed the correlation between HOXC13 expression and DNA damage repair levels in PCa. Correlation analysis demonstrated that HOXC13 expression was positively correlated with DNA damage repair levels, suggesting that high HOXC13 expression promotes DNA damage repair in PCa cells (Fig. 4E).

### Silencing HOXC13 exerts anti-tumor effects in vitro

To further clarify the role of HOXC13 in PCa, we performed reverse validation by gene silencing. Since HOXC13 is a key driver of CRPC-AR subtype, we proposed to select PCa cell lines with high or null AR expression for the study to observe whether the effect of HOXC13 on PCa cell function possesses AR expression dependence. The transcriptional expression levels of HOXC13 in different PCa cell lines were observed using THE HUMAN PROTEIN ATLAS (<https://www.proteinatlas.org/>), and combined with protein expression validation (Additional file 2: Fig. S2A and B), the 22RV1 (HOXC13<sup>+</sup>/AR<sup>+</sup>) and DU145 (HOXC13<sup>+</sup>/AR<sup>-</sup>) cell lines were finally selected for subsequent experiments. To eliminate false positive results caused by off-target effects, we selected two siRNAs with the

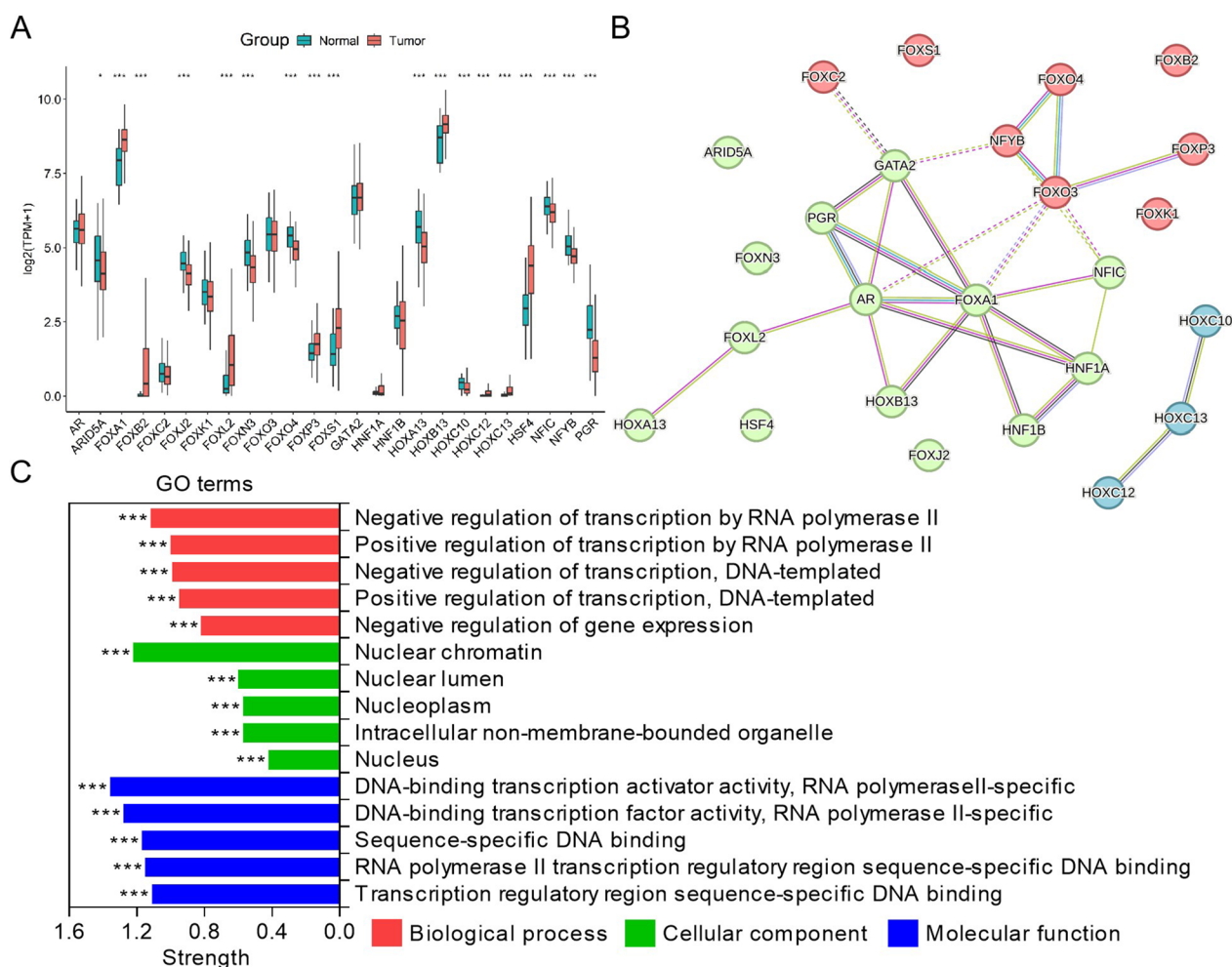


**Fig. 1** Expression properties of 25 TFs in PCa. **A** Expression of 25 TFs in PCa tissues (n = 498) and paracancerous tissues (n = 52). **B** Interaction and clustering among 25 TFs. **C** GO enrichment of 25 TFs. (\*P < 0.05, \*\*P < 0.01, \*\*\*P < 0.001)

best interference effect for comparison. Combining the results of qRT-PCR and WB, we found that both siHOXC13-3 and HOXC13-4 had a more stable interference effect in 22RV1 and DU145 cells, which can be used for subsequent experiments (Additional file 3: Fig. S3A–F). Cell function assays showed that silencing HOXC13 significantly inhibited 22RV1 cell proliferation, migration and invasion, and promoted cell apoptosis (Fig. 5A–G). The same results were shown for DU145 cell function (Additional file 4: Fig. S4A–G). These results indicate that the effects of HOXC13 on PCa cell function are not dependent on AR expression. HOXC13 plays an important mediating role in PCa development, suggesting that HOXC13 is an oncogene for PCa.

**Silencing HOXC13 induces cellular DNA damage and activates cGAS/STING/ IRF3 pathway**

Since HOXC13 mediates cellular DNA damage repair, we speculate that silencing HOXC13 may disrupt DNA repair mechanisms and exacerbate DNA damage. When DNA damage reaches a certain level, numerous broken double-stranded DNA (dsDNA) is released into cytoplasm and accumulates. cGAS/STING/IRF3, as a novel DNA damage response pathway, can be activated by cytoplasmic dsDNA to regulate cell function and immune activity. IF staining revealed that silencing HOXC13 significantly promoted dsDNA accumulation in 22RV1 cells (Fig. 6A). When cellular DNA is damaged, serine 139 on H2AX undergoes phosphorylation modification to form γH2AX, which is a biomarker to

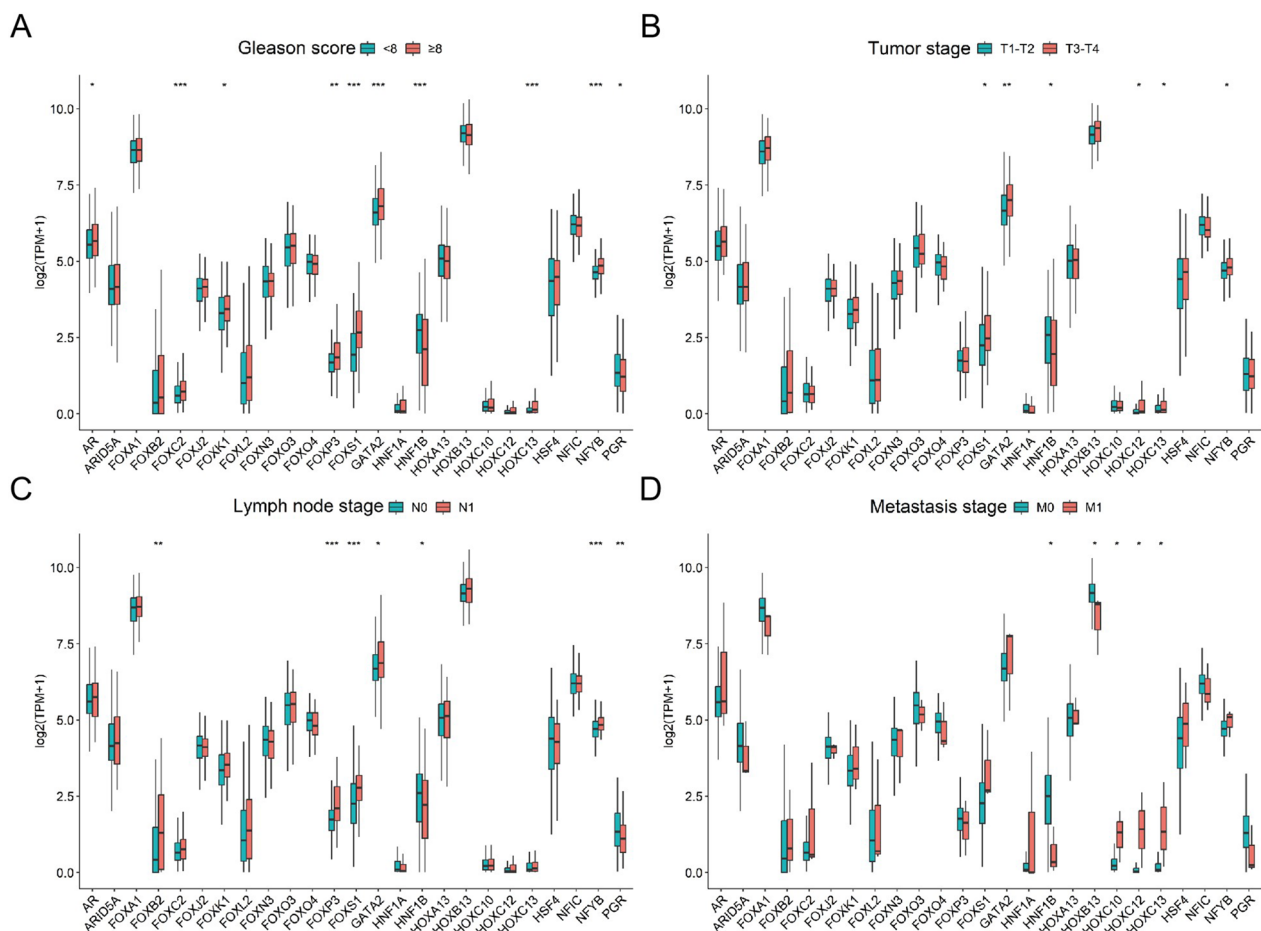


**Fig. 2** Correlation between 25 TFs and clinical features in PCa. **A** Expression of 25 TFs in PCa patients with GS <math>< 8</math> ( $n = 285$ ) and GS  $\geq 8$  ( $n = 196$ ). **B** Expression of 25 TFs in PCa patients with T1–T2 stage ( $n = 186$ ) and T3–T4 stage ( $n = 288$ ). **C** Expression of 25 TFs in PCa patients with N0 stage ( $n = 337$ ) and N1 stage ( $n = 75$ ). **D** Expression of 25 TFs in PCa patients with M0 stage ( $n = 440$ ) and M1 stage ( $n = 3$ ). (\* $P < 0.05$ , \*\* $P < 0.01$ , \*\*\* $P < 0.001$ )

measure the degree of DNA damage. WB results further demonstrated that silencing HOXC13 significantly inhibited its nuclear translocation and up-regulated  $\gamma$ H2AX in 22RV1 cells (Fig. 6B and C). To validate the mediated relationship between HOXC13 and cGAS/STING/IRF3 pathway, reverse proof was performed using the specific cGAS inhibitor RU.521. Pre-experiments showed that 20  $\mu$ M RU.521 was not toxic to 22RV1 and DU145 cells and could effectively inhibit cGAS expression (Additional file 5: Fig. S5A–D). Therefore, this dose was selected for subsequent experiments. Pathway validation demonstrated that RU.521 (a specific cGAS inhibitor) could attenuate silencing HOXC13-induced cGAS up-regulation and STING and IRF3 phosphorylation in 22RV1 cells (Fig. 6D and E). Similarly, we obtained consistent results on DU145 cell experiments (Additional file 6: Fig. S6A–E). These results indicated that silencing HOXC13 induces DNA

damage and activates cGAS/STING/IRF3 pathway in PCa cells.

#### High HOXC13 expression suppresses anti-tumor immune response

cGAS/STING/IRF3 pathway is known to play a critical role in innate immune response and anti-tumor immunity. Therefore, whether HOXC13 mediates the alteration of TIME in PCa aroused our curiosity. Immune infiltration analysis revealed that various immune cells were infiltrated in TIME and that PCa patients with high HOXC13 expression were accompanied by low infiltration of tumor-killing immune cells ( $\gamma\delta$  T cells and plasma cells) and monocytes, while promoting high infiltration of tumor promoting immune cells (M2 macrophages) (Fig. 7A and B). To verify the effects of HOXC13 on immune response, we examined the transcriptional expression levels of IFN- $\beta$ , a downstream gene of IRF3,

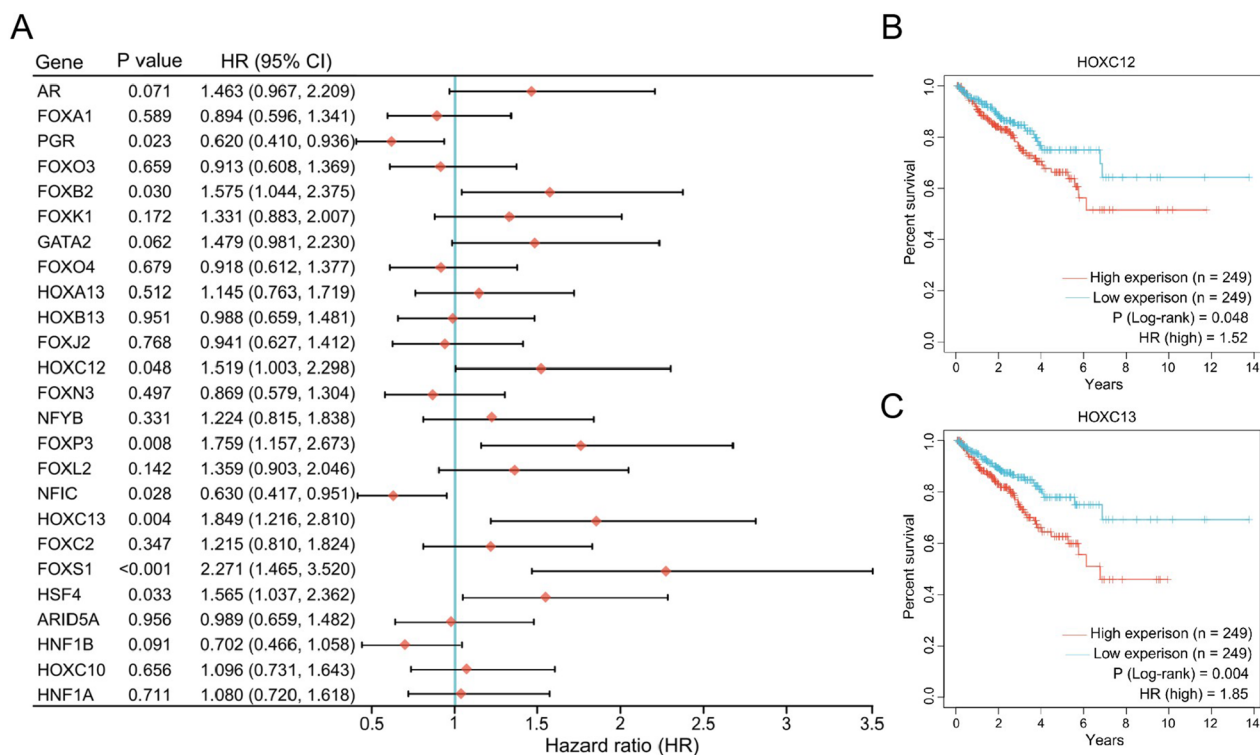


**Fig. 3** Prognostic characterization of 25 TFs in PCa. **A** Risk levels of 25 TFs in PCa. **B** OS of PCa patients with low (n = 249) and high (n = 249) HOXC13 expression (P = 0.048, HR = 1.52). **C** OS of PCa patients with low (n = 249) and high (n = 249) HOXC13 expression (P = 0.004, HR = 1.85)

and some immune-related chemokines (CCL2, CCL5 and CXCL10). qRT-PCR results showed that silencing HOXC13 significantly up-regulated IFN-β, CCL2, CCL5 and CXCL10 in 22RV1 and DU145 cells (Fig. 7C and D). These results suggest that HOXC13 can remodel the TIME in PCa, that high HOXC13 expression suppresses anti-tumor immune response, and that HOXC13 may be a potential target for immunotherapy.

**Discussion**

PCa development involves dysregulation of key TFs expression or disruption of transcriptional network following gene mutation [22]. Based on 25 key TFs in CRPC-AR, we comprehensively assessed their characterization in PCa progression. Bioinformatics results revealed that 25 TFs were aberrantly expressed in PCa, particularly in FOX family (FOXA1, FOXO3, FOXB2, FOXK1, FOXO4, FOXJ2, FOXN3, FOXP3, FOXL2, FOXC2 and FOXS1) and HOX family (HOXA13, HOXB13, HOXC10, HOXC12 and HOXC13). Involvement of FOX family in PCa formation and metastasis has been reported in numerous cases, of which FOXA1 is essential in regulating AR-mediated tumor development, and other FOX members have been confirmed to play regulatory roles in progression

of various cancers [23]. PPI analysis also indicated the central role of FOX family in 25 TFs. However, we were surprised to find HOXC10, HOXC12 and HOXC13 in HOX family as an independent cluster whose role in PCa has rarely been reported, which aroused our strong concern.

HOX gene encodes a family of transcription factors containing homologous structural domains (containing four clusters A, B, C and D) that play important roles in early embryo, including establishment of cellular and tissue identity, as well as regulation of cellular proliferation, differentiation, as well as regulation of cellular survival [24]. HOX proteins have non-transcriptional activity and are involved in regulation of various processes, such as DNA replication and repair, mRNA translation and protein degradation [25]. Numerous studies have confirmed that most of HOX genes are oncogenic and support malignant phenotypes, such as cervical cancer, colon cancer and esophageal cancer [26–28]. Further analysis revealed that HOX family was closely associated with clinical features of PCa, among which HOXC13 was particularly prominent and highly correlated with GS, T stage and M stage. Tissue microarray demonstrated that HOXC13 was highly expressed in PCa tissues and was more overexpressed in patients with high pathological grade. Survival analysis also revealed



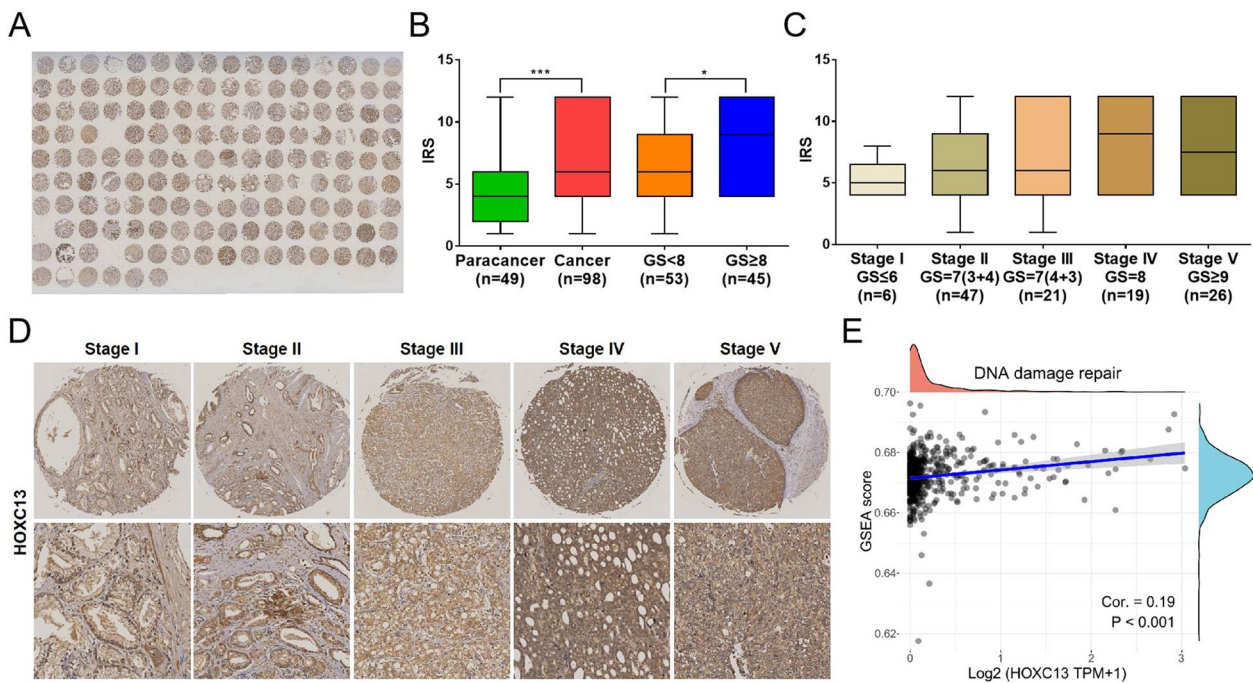


**Fig. 4** Expression of HOXC13 in PCa tissues. **A** Full view of IHC staining for HOXC13 expression (147 cases available after excluding 3 cases without staining). **B** Expression statistics of HOXC13 in paracancerous tissues (n = 49) and PCa tissues (n = 98) and PCa tissues with GS < 8 (n = 53) and GS ≥ 8 (n = 45). **C** Expression statistics of HOXC13 in PCa tissue with stage I (n = 6), stage II (n = 47), stage III (n = 21), stage IV (n = 19) and stage V (n = 26). **D** Expression of HOXC13 in PCa tissues with different tumor stages (stage I to stage V). **E** Correlation between HOXC13 expression and DNA damage repair levels (r = 0.19, P < 0.001). (\*P < 0.05, \*\*\*\*P < 0.001)

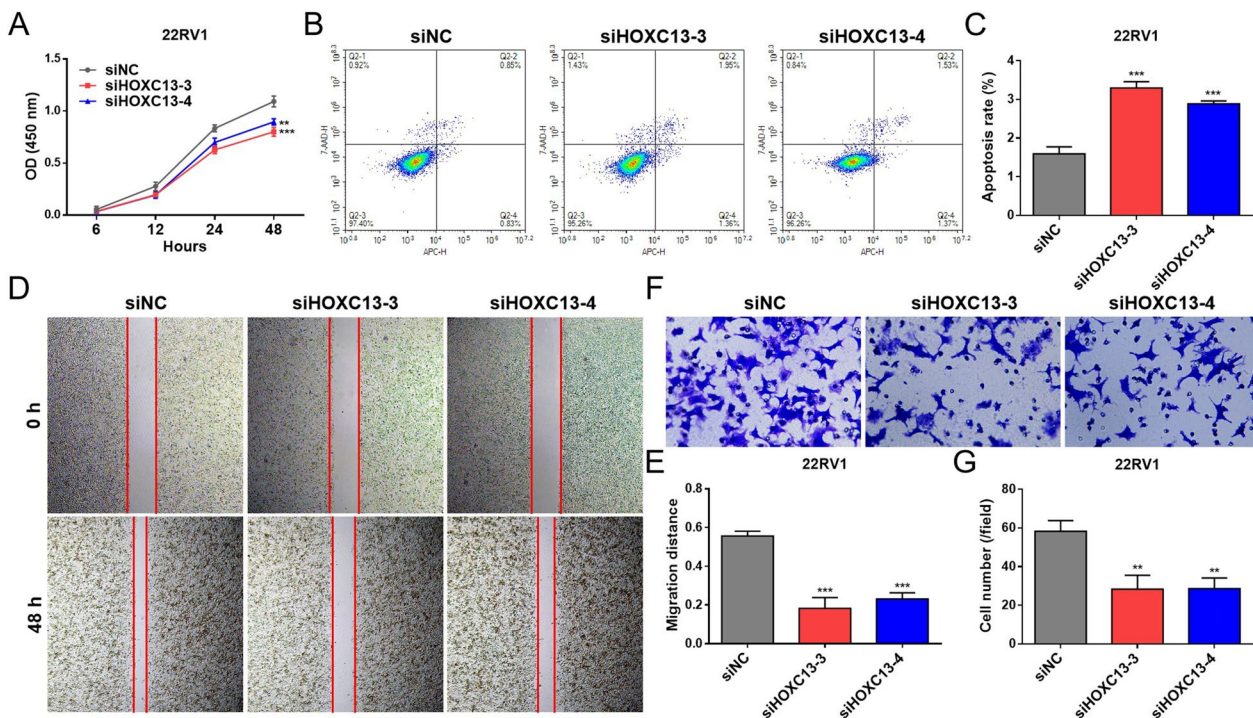


**Fig. 5** Effects of silencing HOXC13 on 22RV1 cell function. **A** Cell proliferation levels at 6, 12, 24 and 48 h. **B** Cell apoptosis levels at 48 h. **C** Statistics of cell apoptosis levels. **D** Cell migration levels at 48 h. **E** Statistics of cell migration levels. **F** Cell invasion levels at 48 h. **G** Statistics of cell invasion levels. (\*P < 0.05, \*\*P < 0.01, \*\*\*P < 0.001)

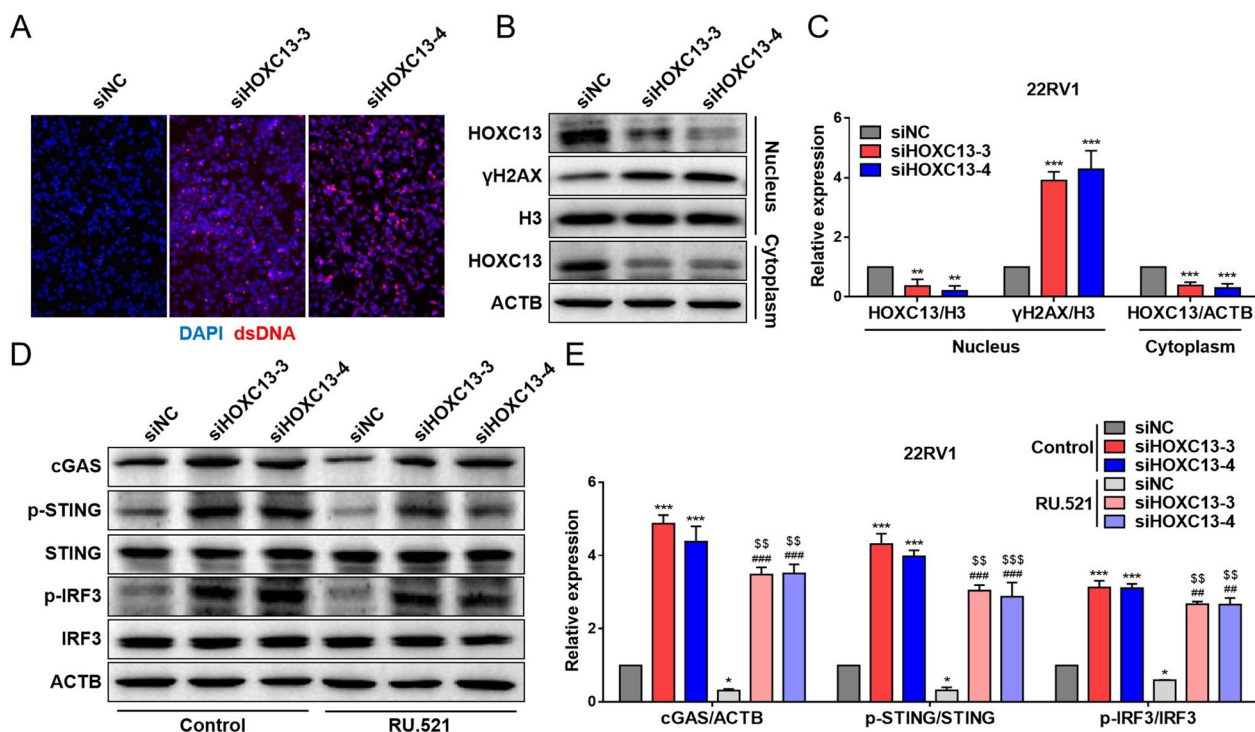


**Fig. 6** Effects of silencing HOXC13 on DNA damage-induced cGAS/STING/IRF3 pathway in 22RV1 cells. **A** Accumulation of dsDNA in cells. **B** Protein bands for nucleus and cytoplasm. **C** Expression statistics of HOXC13 and  $\gamma$ H2AX proteins. **D** Protein bands for cytoplasm. **E** Expression statistics of cGAS, p-STING, STING, p-IRF3 and IRF3 proteins. (vs. siNC group: \* $P < 0.05$ , \*\* $P < 0.01$ , \*\*\* $P < 0.001$ ; vs. siHOXC13-3 group: ### $P < 0.001$ ; vs. siHOXC13-4 group:  $^{SS}P < 0.01$ ,  $^{SSS}P < 0.001$ )

that high HOXC13 expression was accompanied by worse prognosis. These results suggest that HOXC13 is an oncogene involved in regulation of PCa progression. Land et al. [29] demonstrated that HOXC13 may be able to differentiate between recurrent and non-recurrent PCa, but its mechanism of action is unknown. In addition, the association of HOXC13 with other cancers has been confirmed. In breast cancer, HOXC13 is specifically overexpressed and has a poor prognosis for patients and was strongly correlated with N stage and M stage [30]. In glioblastoma, HOXC13 is an important diagnostic and prognostic biomarker [31]. In vitro experiments further demonstrated the important regulatory role of HOXC13 in PCa cell function, silencing HOXC13 significantly inhibited cell proliferation, migration and invasion, and promoted cell apoptosis. These results are consistent with its role in other cancer cells. In non-small cell lung cancer, silencing HOXC13 counteracts HOXC-AS2 overexpression-induced increases in cell proliferation and migration and decreases in cell apoptosis [32]. In cervical cancer, HOXC13 promotes cell proliferation, migration, invasion and glycolysis by regulating  $\beta$ -catenin/c-Myc pathway [33]. These results suggest a high involvement of HOXC13 in PCa progression.

HOXC family is important molecules that mediate DNA damage repair [34]. As a member of the HOXC family, HOXC13 is most likely to be involved in DNA repair mechanism, as verified by gene-pathway correlation analysis. Further assays revealed that silencing HOXC13 promoted dsDNA accumulation and recruited  $\gamma$ H2AX into nucleus. These results suggest that HOXC13 mediates DNA damage repair in PCa cells. Recent studies have revealed that the innate immune system pathway, cGAS/STING/IRF3, plays a critical role in DNA damage response and immune regulation in various cancers [35–37]. Silencing HOXC13 disrupts cellular DNA repair mechanisms, exacerbates DNA damage and releases dsDNA into cytoplasm. Numerous cytoplasmic dsDNA can be sensed by cGAS to recruit STING anchored in endoplasmic reticulum and triggers phosphorylation activity of IRF3, leading to downstream biological responses. Detection of cGAS/STING/IRF3 pathway-related molecules confirmed the above speculations. Our study establishes a link between HOXC13 and DNA damage-induced cGAS/STING/IRF3 pathway for the first time, which provides novel molecular targets for PCa therapy.

Clinically, ADT remains the basic treatment for advanced PCa. ADT drugs include androgen synthesis

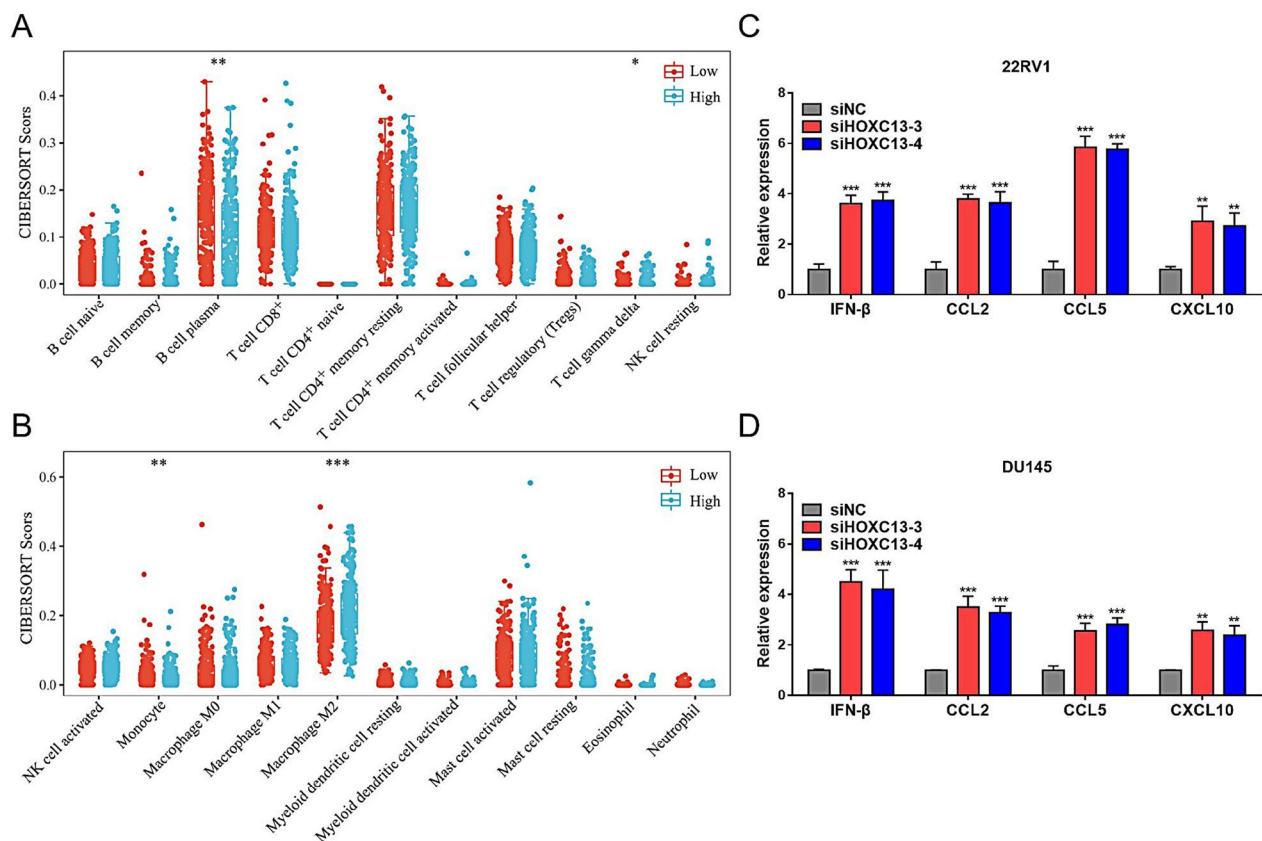


**Fig. 7** Correlation between HOXC13 expression and immune infiltration in PCa. **A, B** Expression of 22 immune cells in low ( $n = 249$ ) and high ( $n = 249$ ) HOXC13 expression groups. **C** Expression statistics of IFN- $\beta$ , CCL2, CCL5 and CXCL10 transcripts in 22RV1 cells. **D** Expression statistics of IFN- $\beta$ , CCL2, CCL5 and CXCL10 transcripts in DU145 cells. (\* $P < 0.05$ , \*\* $P < 0.01$ , \*\*\* $P < 0.001$ )

inhibitors (like Abiraterone), AR inhibitors (like Enzalutamide) and novel AR-targeted drugs (like Apalutamide) [38]. Although ADT is initially effective, it will inevitably progress to CRPC. For AR-dependent CRPC, ADT induces mutations in PCa cells so that they can continue to grow at extremely low concentrations of androgens. These variants include acquired high AR expression or mutation, androgen-independent AR activation, up-regulation of steroid synthase expression and sustained high AR expression in a non-glandular-dependent manner [39]. For AR-independent CRPC, which is inherently insensitive to ADT drugs, resistance can be maintained without AR expression relying on the activation of other signaling pathways (like PI3K/Akt/mTOR and Wnt/ $\beta$ -catenin pathways) [40, 41]. Therefore, ADT efficacy is limited by AR status. Our study found that silencing HOXC13 exerted anti-PCa effects in an AR-independent manner, suggesting a degree of superiority over ADT. Moreover, AR expression unaffected HOXC13-mediated cGAS/STING/IRF3 pathway activation. As the most active molecule in cGAS signaling, STING engages in the

regulation of drug resistance in various cancers. For example, pharmacological STING activation is a potential alternative to overcome drug resistance in melanoma [42]. Recent studies have found that CRPC patients resistant to Abiraterone and Enzalutamide have higher IL-6 levels [43]. In addition, IL-6-induced STAT3 activation promotes CRPC transformation, ADT resistance and Gankyrin expression, leading to formation of the Gankyrin/NONO/AR/HMGB1/IL-6/STAT3 positive feedback signaling pathway, in which STAT3 is the most important transduction molecule [44, 45]. Interestingly, STING activation overcomes STAT3-mediated immunosuppression and adaptive resistance to PARP inhibition [46]. Although there is lack of evidence related to HOXC13-mediated ADT resistance, these studies suggest that it is feasible to inhibit ADT resistance based on activation of STING signaling. Overall, these studies provide guidance for clinical combination therapy (especially with ADT) targeting HOXC13 and its downstream molecules.

In recent years, immunotherapy by modulating the immune function of TME has shown favorable

efficacy in various cancers, but limited efficacy in PCa [47]. Therefore, it is necessary to investigate the role of HOXC13 in regulating TIME in PCa. Immune infiltration analysis revealed that TIME was suppressed in PCa patients with high HOXC13 expression, accompanied by low infiltration of  $\gamma\delta$  T cells, plasma cells and monocytes, and high infiltration of M2 macrophages.  $\gamma\delta$  T cells are T cells that perform innate immune function, both killing cancer cells and recognizing cancer antigens. The immune response of  $\gamma\delta$  T cells is biased towards type I immunity and kills tumor cells mainly by producing granzyme B and perforin [48]. Further studies found that silencing HOXC13 significantly increased IFN- $\beta$ , CCL2, CCL5 and CXCL10 production, which are downstream genes known to be transcriptionally activated by IRF3 and play important regulatory roles in the modulation of immune cell function [49–51].  $\gamma\delta$  T cells can be activated by IFN- $\beta$  and CXCL10 induced in TME to exert cytotoxic effects [52]. In addition, IFN- $\beta$  can partially activate B cells to mediate plasma cell formation and participate in humoral immunity [53]. CCL2 and CCL5 can recruit monocytes to migrate toward tumor foci [54, 55]. In addition to phagocytosis, monocytes can be further induced to differentiate into macrophages, of which M2 macrophages are critical in assisting cancer cells to generate immune escape [56]. These results suggest that HOXC13 has promising application value in mediating anti-tumor immune response and can be used as a novel immunotherapeutic target.

In conclusion, our study revealed HOXC13 as a novel pro-PCa gene that regulates PCa progression by mediating DNA damage-induced cGAS/STING/IRF3 pathway. In addition, HOXC13 can remodel TIME by regulating transcription of immune factors IFN- $\beta$ , CCL2, CCL5 and CXCL10.

#### Abbreviations

PCa	Prostate cancer
PRAD	Prostate adenocarcinoma
CRPC	Castration-resistant prostate cancer
ADT	Androgen deprivation therapy
TFs	Transcription factors
TME	Tumor microenvironment
TIME	Tumor immune microenvironment
ATAC-seq	Transposase-accessible chromatin sequencing
RNA-seq	RNA sequencing
TCGA	The Cancer Genome Atlas
cBioPortal	CBio Cancer Genomics Portal
FPKM	Fragments per kilobase per million
TPM	Transcripts per million
GS	Gleason score
T	Tumor
N	Lymph node
M	Metastasis
dsDNA	Broken double-stranded DNA
PPI	Protein–protein interaction
GO	Gene ontology
FDR	False discovery rate

OS	Overall survival
HR	Hazard ratio
CI	Confidence interval
siRNAs	Small interfering RNAs
IHC	Immunohistochemistry
IF	Immunofluorescence
qRT-PCR	Quantitative reverse transcriptase PCR
WB	Western blot
AR	Androgen receptor
HOXC13	Homeobox C13
$\gamma$ H2AX	Gamma H2A histone family member X
H3	Histone H3
cGAS	Cyclic GMP-AMP synthase
STING	Stimulator of interferon genes
p-STING	Phosphorylated STING
IRF3	Interferon regulatory factor 3
p-IRF3	Phosphorylated IRF3
IFN- $\beta$	Interferon-beta
CCL2	C-C motif chemokine ligand 2
CCL5	C-C motif chemokine ligand 5
CXCL10	C-X-C motif chemokine ligand 10
ACTB	Actin beta

#### Supplementary Information

The online version contains supplementary material available at <https://doi.org/10.1186/s12967-023-04743-x>.

**Additional file 1: Figure S1.** Co-expression correlation among 25 TFs.

**Additional file 2: Figure S2.** Expression of AR and HOXC13 in 22RV1 and DU145 cells. (A) Protein bands for cells. (B) Expression statistics of AR and HOXC13 proteins. (\*\*P < 0.001).

**Additional file 3: Figure S3.** Validation of silencing efficiency for siRNAs targeting HOXC13. (A) Expression statistics of HOXC13 transcript in 22RV1 cells. (B) Protein bands for 22RV1 cells. (C) Expression statistics of HOXC13 protein in 22RV1 cells. (D) Expression statistics of HOXC13 transcript in DU145 cells. (E) Protein bands for DU145 cells. (F) Expression statistics of HOXC13 protein in DU145 cells. (\*P < 0.05, \*\*P < 0.01, \*\*\*P < 0.001).

**Additional file 4: Figure S4.** Effects of silencing HOXC13 on DU145 cell function. (A) Cell proliferation levels at 6, 12, 24 and 48 h. (B) Cell apoptosis levels at 48 h. (C) Statistics of cell apoptosis levels. (D) Cell migration levels at 48 h. (E) Statistics of cell migration levels. (F) Cell invasion levels at 48 h. (G) Statistics of cell invasion levels. (\*P < 0.05, \*\*P < 0.01, \*\*\*P < 0.001).

**Additional file 5: Figure S5.** Screening for optimal dose of the specific cGAS inhibitor RU.521. (A) Effect of different doses of RU.521 on 22RV1 cell viability. (B) Effect of different doses of RU.521 on DU145 cell viability. (C) Protein bands for cells. (D) Expression statistics of cGAS proteins. (vs. 0  $\mu$ M RU.521 group in 22RV1 cells: \*P < 0.05, \*\*P < 0.01, \*\*\*P < 0.001; vs. 0  $\mu$ M RU.521 group in DU145 cells: \*P < 0.05, #P < 0.01, ###P < 0.001).

**Additional file 6: Figure S6.** Effects of silencing HOXC13 on DNA damage-induced cGAS/STING/IRF3 pathway in DU145 cells. (A) Accumulation of dsDNA in cells. (B) Protein bands for nucleus and cytoplasm. (C) Expression statistics of HOXC13 and  $\gamma$ H2AX proteins. (D) Protein bands for cytoplasm. (E) Expression statistics of cGAS, p-STING, STING, p-IRF3 and IRF3 proteins. (vs. siNC group: \*P < 0.05, \*\*P < 0.01, \*\*\*P < 0.001; vs. siHOXC13-3 group: ###P < 0.001; vs. siHOXC13-4 group: \$\$\$P < 0.01, \$\$\$P < 0.001).

#### Acknowledgements

Thanks to all participants involved in this research.

#### Author contributions

ML, GB and YC: Conceptualization, methodology, investigation, writing—original draft. QX, JiahongC, JiaC and QC: Investigation. WZ: Conceptualization, supervision, project administration, funding acquisition. XZ: Supervision, project administration, funding acquisition. All authors contributed to manuscript revision, read, and approved the submitted version.

### Funding

This study was supported by grant from Natural Science Foundation of Guangdong Province, China (Grant Nos. 2021A1515011088, 2021A1515012106) and Guangdong Medical Science and Technology Research Fund Project of China (B2022332, B2020127, B2023213).

### Availability of data and materials

The data presented in this study are available on request from the corresponding authors.

### Declarations

#### Ethics approval and consent to participate

Not applicable.

#### Consent for publication

Not applicable.

#### Competing interests

The authors declare that they have no competing interests.

### Author details

<sup>1</sup>School of Medicine, Jinan University, Guangzhou 510632, Guangdong, China. <sup>2</sup>Department of Urology, Huizhou Municipal Central Hospital, Huizhou 516001, China. <sup>3</sup>Guangdong Provincial Key Laboratory of Molecular Target & Clinical Pharmacology, the NMPA and State Key Laboratory of Respiratory Disease, Guangzhou Medical University, Guangzhou 511436, People's Republic of China. <sup>4</sup>Department of Urology, The Second People's Hospital of Foshan, Affiliated Foshan Hospital of Southern Medical University, Foshan 528000, China.

Received: 7 September 2023 Accepted: 20 November 2023

Published online: 06 December 2023

### References

- Pinsky PF, Parnes H. Screening for prostate cancer. *N Engl J Med*. 2023;388(15):1405–14.
- Seibert TM, Garraway IP, Plym A, Mahal BA, Giri V, Jacobs MF, Cheng HH, Loeb S, Helfand BT, Eeles RA, Morgan TM. Genetic risk prediction for prostate cancer: implications for early detection and prevention. *Eur Urol*. 2023;83(3):241–8.
- Desai K, McManus JM, Sharifi N. Hormonal therapy for prostate cancer. *Endocr Rev*. 2021;42(3):354–73.
- Shafi AA, Yen AE, Weigel NL. Androgen receptors in hormone-dependent and castration-resistant prostate cancer. *Pharmacol Ther*. 2013;140(3):223–38.
- Labrecque MP, Coleman IM, Brown LG, True LD, Kollath L, Lakely B, Nguyen HM, Yang YC, da Costa RMG, Kaipainen A, Coleman R, Higano CS, Yu EY, Cheng HH, Mostaghel EA, Montgomery B, Schweizer MT, Hsieh AC, Lin DW, Corey E, Nelson PS, Morrissey C. Molecular profiling stratifies diverse phenotypes of treatment-refractory metastatic castration-resistant prostate cancer. *J Clin Invest*. 2019;129(10):4492–505.
- Ge R, Wang Z, Montironi R, Jiang Z, Cheng M, Santoni M, Huang K, Masari F, Lu X, Cimadamore A, Lopez-Beltran A, Cheng L. Epigenetic modulations and lineage plasticity in advanced prostate cancer. *Ann Oncol*. 2020;31(4):470–9.
- Wang KC, Chang HY. Epigenomics: technologies and applications. *Circ Res*. 2018;122(9):1191–9.
- Tang F, Xu D, Wang S, Wong CK, Martinez-Fundichely A, Lee CJ, Cohen S, Park J, Hill CE, Eng K, Bareja R, Han T, Liu EM, Palladino A, Di W, Gao D, Abida W, Beg S, Pua L, Meneses M, de Stanchina E, Berger MF, Gopalan A, Dow LE, Mosquera JM, Beltran H, Sternberg CN, Chi P, Scher HI, Sboner A, Chen Y, Khurana E. Chromatin profiles classify castration-resistant prostate cancers suggesting therapeutic targets. *Science*. 2022;376(6596):eabe1505.
- Teng M, Zhou S, Cai C, Lupien M, He HH. Pioneer of prostate cancer: past, present and the future of FOXA1. *Protein Cell*. 2021;12(1):29–38.
- Chen F, Xiong W, Dou K, Ran Q. Knockdown of FOXC1 suppresses proliferation, migration, and invasion in prostate cancer cells. *Oncol Res*. 2017;25(8):1261–7.
- Rodriguez-Bravo V, Carceles-Cordon M, Hoshida Y, Cordon-Cardo C, Galsky MD, Domingo-Domenech J. The role of GATA2 in lethal prostate cancer aggressiveness. *Nat Rev Urol*. 2017;14(1):38–48.
- Luo Z, Rhie SK, Lay FD, Farnham PJ. A prostate cancer risk element functions as a repressive loop that regulates HOXA13. *Cell Rep*. 2017;21(6):1411–7.
- Paranjape AN, Soundararajan R, Werden SJ, Joseph R, Taube JH, Liu H, Rodriguez-Canales J, Sphyris N, Wistuba I, Miura N, Dhillon J, Mahajan N, Mahajan K, Chang JT, Ittmann M, Maity SN, Logothetis C, Tang DG, Mani SA. Inhibition of FOXC2 restores epithelial phenotype and drug sensitivity in prostate cancer cells with stem-cell properties. *Oncogene*. 2016;35(46):5963–76.
- Lv S, Wen H, Shan X, Li J, Wu Y, Yu X, Huang W, Wei Q. Loss of KMT2D induces prostate cancer ROS-mediated DNA damage by suppressing the enhancer activity and DNA binding of antioxidant transcription factor FOXO3. *Epigenetics*. 2019;14(12):1194–208.
- Lu X, Fong KW, Gritsina G, Wang F, Baca SC, Brea LT, Berchuck JE, Spisak S, Ross J, Morrissey C, Corey E, Chandel NS, Catalona WJ, Yang X, Freedman ML, Zhao JC, Yu J. HOXB13 suppresses de novo lipogenesis through HDAC3-mediated epigenetic reprogramming in prostate cancer. *Nat Genet*. 2022;54(5):670–83.
- Wu L, Yi B, Wei S, Rao D, He Y, Naik G, Bae S, Liu XM, Yang WH, Sonpavde G, Liu R, Wang L. Loss of FOXP3 and TSC1 accelerates prostate cancer progression through synergistic transcriptional and posttranslational regulation of c-MYC. *Cancer Res*. 2019;79(7):1413–25.
- Lu W, Sun J, Zhou H, Wang F, Zhao C, Li K, Fan C, Ding G, Wang J. HNF1B inhibits cell proliferation via repression of SMAD6 expression in prostate cancer. *J Cell Mol Med*. 2020;24(24):14539–48.
- Kao KC, Vilbois S, Tsai CH, Ho PC. Metabolic communication in the tumour-immune microenvironment. *Nat Cell Biol*. 2022;24(11):1574–83.
- Khalaf K, Hana D, Chou JT, Singh C, Mackiewicz A, Kaczmarek M. Aspects of the tumor microenvironment involved in immune resistance and drug resistance. *Front Immunol*. 2021;12: 656364.
- Fan J, To KKW, Chen ZS, Fu L. ABC transporters affects tumor immune microenvironment to regulate cancer immunotherapy and multidrug resistance. *Drug Resist Updat*. 2023;66: 100905.
- Huang X, Wang L, Guo H, Zhang W, Shao Z. Single-cell transcriptomics reveals the regulative roles of cancer associated fibroblasts in tumor immune microenvironment of recurrent osteosarcoma. *Theranostics*. 2022;12(13):5877–87.
- Labbé DP, Brown M. transcriptional regulation in prostate cancer. *Cold Spring Harb Perspect Med*. 2018;8(11): a030437.
- Wang J, Li W, Zhao Y, Kang D, Fu W, Zheng X, Pang X, Du G. Members of FOX family could be drug targets of cancers. *Pharmacol Ther*. 2018;181:183–96.
- Mallo M, Wellik DM, Deschamps J. Hox genes and regional patterning of the vertebrate body plan. *Dev Biol*. 2010;344(1):7–15.
- Rezsohazy R, Saurin AJ, Maurel-Zaffran C, Graba Y. Cellular and molecular insights into Hox protein action. *Development*. 2015;142(7):1212–27.
- Zhang Z, Peng J, Li B, Wang Z, Wang H, Wang Y, Hong L. HOXA1 promotes aerobic glycolysis and cancer progression in cervical cancer. *Cell Signal*. 2023;109: 110747.
- Cui M, Chen M, Shen Z, Wang R, Fang X, Song B. LncRNA-UCA1 modulates progression of colon cancer through regulating the miR-28-5p/HOXB3 axis. *J Cell Biochem*. 2019;120(5):6926–36.
- Li HM, Yu YK, Liu Q, Wei XF, Zhang J, Zhang RX, Sun HB, Wang ZF, Xing WQ, Li Y. LncRNA SNHG1 regulates the progression of esophageal squamous cell cancer by the miR-204/HOXC8 Axis. *Oncotargets Ther*. 2020;13:757–67.
- Komisarof J, McCall M, Newman L, Bshara W, Mohler JL, Morrison C, Land H. A four gene signature predictive of recurrent prostate cancer. *Oncotarget*. 2017;8(2):3430–40.
- Li C, Cui J, Zou L, Zhu L, Wei W. Bioinformatics analysis of the expression of HOXC13 and its role in the prognosis of breast cancer. *Oncol Lett*. 2020;19(1):899–907.
- Yu M, Yu S, Zhou W, Yi B, Liu Y. HOXC6/8/10/13 predict poor prognosis and associate with immune infiltrations in glioblastoma. *Int Immunopharmacol*. 2021;101(Pt A): 108293.

32. Liu B, Li J, Li JM, Liu GY, Wang YS. HOXC-AS2 mediates the proliferation, apoptosis, and migration of non-small cell lung cancer by combining with HOXC13 gene. *Cell Cycle*. 2021;20(2):236–46.
33. Dai M, Song J, Wang L, Zhou K, Shu L. HOXC13 promotes cervical cancer proliferation, invasion and Warburg effect through  $\beta$ -catenin/c-Myc signaling pathway. *J Bioenerg Biomembr*. 2021;53(5):597–608.
34. Zhou T, Fu H, Dong B, Dai L, Yang Y, Yan W, Shen L. HOXB7 mediates cisplatin resistance in esophageal squamous cell carcinoma through involvement of DNA damage repair. *Thorac Cancer*. 2020;11(11):3071–85.
35. Riederer S, Del Canizo A, Navas J, Peter MG, Link EK, Sutter G, Rojas JJ. Improving poxvirus-mediated antitumor immune responses by deleting viral cGAMP-specific nuclease. *Cancer Gene Ther*. 2023;30(7):1029–39.
36. Lu X, Wang X, Cheng H, Wang X, Liu C, Tan X. Anti-triple-negative breast cancer metastasis efficacy and molecular mechanism of the STING agonist for innate immune pathway. *Ann Med*. 2023;55(1):2210845.
37. Kessler N, Viehmann SF, Krollmann C, Mai K, Kirschner KM, Luksch H, Kotagiri P, Böhner AMC, Huuugen D, de Oliveira Mann CC, Otten S, Weiss SAI, Zillinger T, Dobrikova K, Jenne DE, Behrendt R, Ablasser A, Bartok E, Hartmann G, Hopfner KP, Lyons PA, Boor P, Rösen-Wolff A, Teichmann LL, Heeringa P, Kurts C, Garbi N. Monocyte-derived macrophages aggravate pulmonary vasculitis via cGAS/STING/IFN-mediated nucleic acid sensing. *J Exp Med*. 2022;219(10):e20220759.
38. Crawford ED, Heidenreich A, Lawrentschuk N, Tombal B, Pompeo ACL, Mendoza-Valdes A, Miller K, Debruyne FMJ, Klotz L. Androgen-targeted therapy in men with prostate cancer: evolving practice and future considerations. *Prostate Cancer Prostatic Dis*. 2019;22(1):24–38.
39. Eisermann K, Wang D, Jing Y, Pascal LE, Wang Z. Androgen receptor gene mutation, rearrangement, polymorphism. *Transl Androl Urol*. 2013;2(3):137–47.
40. Shorning BY, Dass MS, Smalley MJ, Pearson HB. The PI3K-AKT-mTOR pathway and prostate cancer: at the crossroads of AR, MAPK, and WNT signaling. *Int J Mol Sci*. 2020;21(12):4507–54.
41. Miyamoto DT, Zheng Y, Wittner BS, Lee RJ, Zhu H, Broderick KT, Desai R, Fox DB, Brannigan BW, Trautwein J, Arora KS, Desai N, Dahl DM, Sequist LV, Smith MR, Kapur R, Wu CL, Shioda T, Ramaswamy S, Ting DT, Toner M, Maheswaran S, Haber DA. RNA-Seq of single prostate CTCs implicates noncanonical Wnt signaling in antiandrogen resistance. *Science*. 2015;349(6254):1351–6.
42. Chipurupalli S, Ganesan R, Dhanabal SP, Kumar MS, Robinson N. Pharmacological STING activation is a potential alternative to overcome drug-resistance in melanoma. *Front Oncol*. 2020;10:758–67.
43. Xu P, Yang JC, Chen B, Nip C, Van Dyke JE, Zhang X, Chen HW, Evans CP, Murphy WJ, Liu C. Androgen receptor blockade resistance with enzalutamide in prostate cancer results in immunosuppressive alterations in the tumor immune microenvironment. *J Immunother Cancer*. 2023;11(5):e006581.
44. Peng G, Wang C, Wang H, Qu M, Dong K, Yu Y, Jiang Y, Gan S, Gao X. Gankyrin-mediated interaction between cancer cells and tumor-associated macrophages facilitates prostate cancer progression and androgen deprivation therapy resistance. *Oncoimmunology*. 2023;12(1):2173422.
45. Zhong S, Huang C, Chen Z, Chen Z, Luo JL. Targeting inflammatory signaling in prostate cancer castration resistance. *J Clin Med*. 2021;10(21):5000–16.
46. Ding L, Wang Q, Martincuks A, Kearns MJ, Jiang T, Lin Z, Cheng X, Qian C, Xie S, Kim HJ, Launonen IM, Färkkilä A, Roberts TM, Freeman GJ, Liu JF, Konstantinopoulos PA, Matulonis U, Yu H, Zhao JJ. STING agonism overcomes STAT3-mediated immunosuppression and adaptive resistance to PARP inhibition in ovarian cancer. *J Immunother Cancer*. 2023;11(1):e005627.
47. Cha HR, Lee JH, Ponnazhagan S. Revisiting immunotherapy: a focus on prostate cancer. *Cancer Res*. 2020;80(8):1615–23.
48. Silva-Santos B, Mensurado S, Coffelt SB.  $\gamma\delta$ T cells: pleiotropic immune effectors with therapeutic potential in cancer. *Nat Rev Cancer*. 2019;19(7):392–404.
49. Ko R, Seo J, Park H, Lee N, Lee SY. Pim1 promotes IFN- $\beta$  production by interacting with IRF3. *Exp Mol Med*. 2022;54(11):2092–103.
50. Ahmad R, Al-Roub A, Kochumon S, Akther N, Thomas R, Kumari M, Koshy MS, Tiss A, Hannun YA, Tuomilehto J, Sindhu S, Rosen ED. The synergy between palmitate and TNF- $\alpha$  for CCL2 production is dependent on the TRIF/IRF3 pathway: implications for metabolic inflammation. *J Immunol*. 2018;200(10):3599–611.
51. Taniguchi H, Caesar R, Chavan SS, Zhan YA, Chow A, Manoj P, Uddin F, Kitai H, Qu R, Hayatt O, Shah NS, Quintanal Villalonga Á, Allaj V, Nguyen EM, Chan J, Michel AO, Mukae H, de Stanchina E, Rudin CM, Sen T. WEE1 inhibition enhances the antitumor immune response to PD-L1 blockade by the concomitant activation of STING and STAT1 pathways in SCLC. *Cell Rep*. 2022;39(7):110814.
52. Liu R, Wu N, Gao H, Liang S, Yue K, Dong T, Dong X, Xu LP, Wang Y, Zhang XH, Liu J, Huang XJ. Distinct activities of  $\gamma\delta$ 1+ T-cells upon different cytomegalovirus reactivation status after haematopoietic transplantation. *Immunology*. 2022;167(3):368–83.
53. Vazquez MI, Catalan-Dibene J, Zlotnik A. B cells responses and cytokine production are regulated by their immune microenvironment. *Cytokine*. 2015;74(2):318–26.
54. Aretz P, Maciaczyk D, Yusuf S, Sorg RV, Hänggi D, Liu H, Liu H, Dakal TC, Sharma A, Bethanabatla R, Neumann S, Maciaczyk J. Crosstalk between  $\beta$ -Catenin and CCL2 drives migration of monocytes towards glioblastoma cells. *Int J Mol Sci*. 2022;23(9):4562–78.
55. Hussen J, Frank C, Düvel A, Koy M, Schuberth HJ. The chemokine CCL5 induces selective migration of bovine classical monocytes and drives their differentiation into LPS-hyporesponsive macrophages in vitro. *Dev Comp Immunol*. 2014;47(2):169–77.
56. Zheng Y, Ren S, Zhang Y, Liu S, Meng L, Liu F, Gu L, Ai N, Sang M. Circular RNA circWWC3 augments breast cancer progression through promoting M2 macrophage polarization and tumor immune escape via regulating the expression and secretion of IL-4. *Cancer Cell Int*. 2022;22(1):264–77.

## Publisher's Note

Springer Nature remains neutral with regard to jurisdictional claims in published maps and institutional affiliations.

Ready to submit your research? Choose BMC and benefit from:

- fast, convenient online submission
- thorough peer review by experienced researchers in your field
- rapid publication on acceptance
- support for research data, including large and complex data types
- gold Open Access which fosters wider collaboration and increased citations
- maximum visibility for your research: over 100M website views per year

At BMC, research is always in progress.

Learn more [biomedcentral.com/submissions](https://biomedcentral.com/submissions)

